IEEE Transactions on Vehicular Technology, Available early online, June 2019
DOI: 10.1109/TVT.2019.2921563

Generalized Hybrid Beamforming for Vehicular Connectivity using THz Massive MIMO

Sherif Adeshina Busari, *Student Member, IEEE*, Kazi Mohammed Saidul Huq, *Senior Member, IEEE*, Shahid Mumtaz, *Senior Member, IEEE*, Jonathan Rodriguez, *Senior Member, IEEE*, Yi Fang, *Member, IEEE* Douglas C. Sicker, Saba Al-Rubaye, *Senior Member, IEEE* and Antonios Tsourdos

***Abstract*—Hybrid beamforming (HBF) array structure has been extensively demonstrated as the practically-feasible architecture for massive MIMO. From the perspectives of spectral efficiency (SE), energy efficiency (EE), cost and hardware complexity, HBF strikes a balanced performance tradeoff when compared to the fully-analog and the fully-digital implementations. Using the HBF architecture, it is possible to realize three different subarray structures, specifically the fully-connected, the sub-connected and the overlapped subarray structures. This paper presents a novel generalized framework for the design and performance analysis of the HBF architecture. A parameter, known as the subarray spacing, is introduced such that varying its value leads to the different subarray configurations and the consequent changes in system performance. Using a realistic power consumption model, we investigate the performance of the generalized HBF array structure in a cellular infrastructure-to-everything (C-I2X) application scenario (involving pedestrian and vehicular users) using the single-path terahertz (THz) channel model. Simulation results are provided for the comparative performance analysis of the different subarray structures. The results show that the overlapped subarray implementation maintains a balanced tradeoff in terms of SE, EE and hardware cost when compared to the popular fully-connected and the sub-connected structures. The overlapped subarray structure, therefore, offers promising potentials for the beyond-5G networks employing THz massive MIMO to deliver ultra-high data rates whilst maintaining a balance in the EE of the network.**

***Index Terms*—Antenna array, B5G, C-I2X, Hybrid beamforming, Massive MIMO, Terahertz, V2X.**

The work of S. A. Busari and K. M. S. Huq was supported by the Fundação para a Ciência e a Tecnologia (FCT), Portugal through Ph.D. Grants under Reference PD/BD/113823/2015 and through Post-Doctoral Grants under Reference SFRH/BPD/110104/2015, respectively. This work is also funded by FCT/MEC through national funds under the project (THz-BEGUN under CMU Portugal call), CMU/ECE/0013/2017 and the European Commission H2020 program under grant agreement no. 815178 (5GENESIS project). *(Corresponding author: Sherif Adeshina Busari.)*

S. A. Busari, K. M. S. Huq, S. Mumtaz and J. Rodriguez are with the Instituto de Telecomunicações, Aveiro, Portugal (e-mail: {sherifbusari, kazi.saidul, smumtaz, jonathan}@av.it.pt).

J. Rodriguez is also with the University of South Wales, Pontypridd, United Kingdom (e-mail: jonathan.rodriguez@southwales.ac.uk).

Y. Fang is with the School of Information Engineering, Guangdong University of Technology, Guangzhou 510006, China and the National Mobile Communications Research Laboratory, Southeast University, Nanjing 210096, China (e-mail: fangyi@gdut.edu.cn).

D. C. Sicker is with the Department of Engineering and Public Policy, and also with the School of Computer Science, Carnegie Mellon University, Pittsburgh, PA USA (e-mail: sicker@cmu.edu).

S. Al-Rubaye and A. Tsourdos are with the School of Aerospace, Transport and Manufacturing, Cranfield University, UK (e-mail: {S.Alrubaye, a.tsourdos}@cranfield.ac.uk).

I. Introduction

THE DATA traffic forecasts for the beyond fifth-generation (B5G) era imply that the available bandwidths in the sub-6 GHz microwave (μWave) bands and the lower end of the millimeter-wave (mmWave) bands (i.e., less than 90 GHz) will be inadequate to meet the data rate demands of users. Next-generation cellular and vehicular applications, for example, are envisaged to require data rates on the order of multi-gigabits-per-second (Gbps) to terabits-per-second (Tbps) on the downlink. For these two domains of mobile wireless connectivity, only the terahertz (THz) bands (0.1-10 THz)[1] can provide the multi-gigahertz (GHz) contiguous bandwidths required to meet the projected throughput demands [1]–[3]. As a result, THz band communication (THzBC) has received considerable attention in the research community in the present decade. This trend is expected to continue as the progress being made in various areas of THzBC (such as electronic components, channel modeling, spectrum allocation, standardization, use cases, etc.) continue to spur further research activities [4], [5].

To enable THzBC, the transmitters (TX) and receivers (RX) must use antenna arrays with a high number of antenna elements (AEs), otherwise referred to as the large scale antenna system (LSAS) or massive multiple-input multiple-output (MIMO) [4]. This is because the free space path loss (FSPL) increases as the carrier frequency (f_c) increases, according to the fundamental Friis equation [6]. Fortunately, a $100\times$ increase in f_c (e.g., from 6 GHz to 0.6 THz) correspondingly leads to a 100-fold reduction in wavelength (λ). As a result, the dimensions of the antenna elements as well as their inter-element spacing become incredibly small (due to their dependence on λ). It thus becomes possible to pack a large number of antenna elements in a physically-limited space thereby enabling massive MIMO [7].

Using appropriate beamforming or precoding[2] techniques, massive MIMO can provide the needed array gains to counter the severe effects of the high path loss (PL) at high frequencies (e.g., mmWave, THz) and thus increase the signal-to-noise ratio (SNR) for user devices. It also provides the

[1]The US Federal Communications Commission has, on 15 March 2019, approved a new category of experimental licenses for frequencies between 95 GHz and 3 THz for THz communications and other applications. https://docs.fcc.gov/public/attachments/DOC-356588A1.pdf

[2]Beamforming is used in its widest meaning, throughout this paper, such that beamforming and precoding refer to exactly the same thing and can be used interchangeably. (cf.: https://ma-mimo.ellintech.se/2017/10/03/what-is-the-difference-between-beamforming-and-precoding/).

opportunity for highly-directional beams to mitigate multi-user interference (MUI). The large arrays can also be leveraged to provide spatial multiplexing gains by transmitting multiple streams so as to boost spectral efficiency (SE) [7]–[9]. The combined benefits from the huge bandwidth in THz as well as the array and multiplexing gains from massive MIMO will lead to significant enhancement in user throughput, quality of experience (QoE) and system capacity. More so, B5G targets green (energy-efficient), soft (self-organizing) and super-fast (ultra-high rate) networks [10]. Thus, energy efficiency (EE) is a critical key performance indicator (KPI) for THz massive MIMO. The research community has thus been investigating different system architectures with a view to identifying the optimal model, not only in terms of the SE-EE performance but also with respect to the hardware requirement, cost and implementation complexity [5], [11], [12].

For massive MIMO, three beamforming architectures have been identified: (i) analog beamforming (ABF), (ii) digital beamforming (DBF) and (iii) hybrid beamforming (HBF) [7], [13]. In the ABF implementation, all the antenna elements are connected to a single radio frequency chain (RFC) via a network of phase shifters (PS). For DBF, each antenna element is connected to a dedicated RFC. The HBF architecture uses a reduced number of RFCs. It divides its structure into two stages: the large-sized ABF stage for increasing array gain and the small-sized DBF stage for mitigating MUI [8], [14], [15]. Comparing the three architectures, HBF maintains a balanced performance between the ABF (with low SE, power consumption, cost and complexity) on the one hand and the DBF (with high SE, power consumption, cost and complexity) on the other. As a result, HBF has been copiously demonstrated as the realistic and practically-feasible array structure for massive MIMO [7], [11]. It is thus the architecture of interest in this paper.

A. Related Works

Focusing on the HBF architecture, different subarray structures can be realized depending on the interconnection among the RF chains, PSs and AEs (i.e., the RF-PS-AE mapping). The three structures that have been proposed in the literature are: (i) the fully-connected structure [7], [11], [14], (ii) the sub-connected structure [11], [13], [14] (also known as the partially-connected or array-of-subarrays [5]) and (iii) the overlapped subarray structure [12], [16]. The performance analyses of these HBF structures have been investigated for diverse scenarios. The authors in [9], [11], [17] considered single-cell, single-user, multi-stream communication while the authors in [8] and [18] analyzed for the single-cell, multi-user, multi-stream system. In [19], the HBF evaluation was extended to the multi-cell, multi-user, multi-stream scenario. However, these evaluations consider the typical cellular deployments with inter-site distances (ISD) ≥ 500 m for the μWave setups and 50-200 m for the mmWave scenarios. Extension to the THz domain with ISDs $\leq$ 10 m, particularly for outdoor applications, is still missing.

In addition, the fully-connected and the sub-connected array structures have received considerable attention in the literature [5], [8], [11]. However, the investigation of the overlapped array structure is rather very limited [12], [16]. More so, the analyses of the HBF structures are usually done in a disjoint manner. To the best knowledge of the authors, no generalized framework is available in the literature for a comprehensive and comparative analysis of the different structures in a unified and systematic manner.

B. Contributions

In this work, we propose a novel generalized framework for the design and analysis of HBF antenna array structures. To the authors' best knowledge, this work is the first to explore the analysis in a generalized fashion. The main contributions and results of this paper are outlined as follows:

- We develop a generalized model for the design and analysis of any HBF array structure or configuration using THz massive MIMO. We outline, in a step-wise manner, the procedures for the design and then we analyze the performance of quintessential configurations comparatively. The evaluation is done using a cellular infrastructure-to-everything (C-I2X) application scenario involving both cellular and vehicular communication.
- Using a realistic power consumption model, we assess the performance of the system not only in terms of the SE and EE but also the power and hardware cost for the network. Different from most existing works, our comprehensive power consumption model includes the TX power, the TX circuit power, RX circuit power as well as the backhaul power. Our results reveal that the backhaul power constitute the largest percentage of the total power consumption in the B5G scenario as ultra-high data rates are exchanged between the TX and the core network. This result is contrary to the situation with relatively low-rate legacy networks where the TX power takes the largest chunk.
- For all subarray structures, the EE-SE performance curves follow the typical quasi-concave (bell-shaped) trend. As the SE increases, the EE increases first, then reaches the optimal value and continues to decrease thereafter. The optimal EE point is critical for the design of energy-efficient networks.
- In between the fully-connected structure with the highest SE and the sub-connected structure with the largest EE, our results show that the overlapped subarray structures offer an exciting window for a balanced performance tradeoff, not only with respect to SE and EE but also the power and hardware costs. Thus, the overlapped configurations can be further harnessed to optimize the performance of future networks.

C. Paper Organization

The remainder of this paper is organized as follows. In Section II, we present the proposed generalized HBF subarray structure, highlighting the design procedures and the practical power consumption model for the analysis. The C-I2X application scenario used in this work is presented in Section III. We describe the system model, THz channel model and the

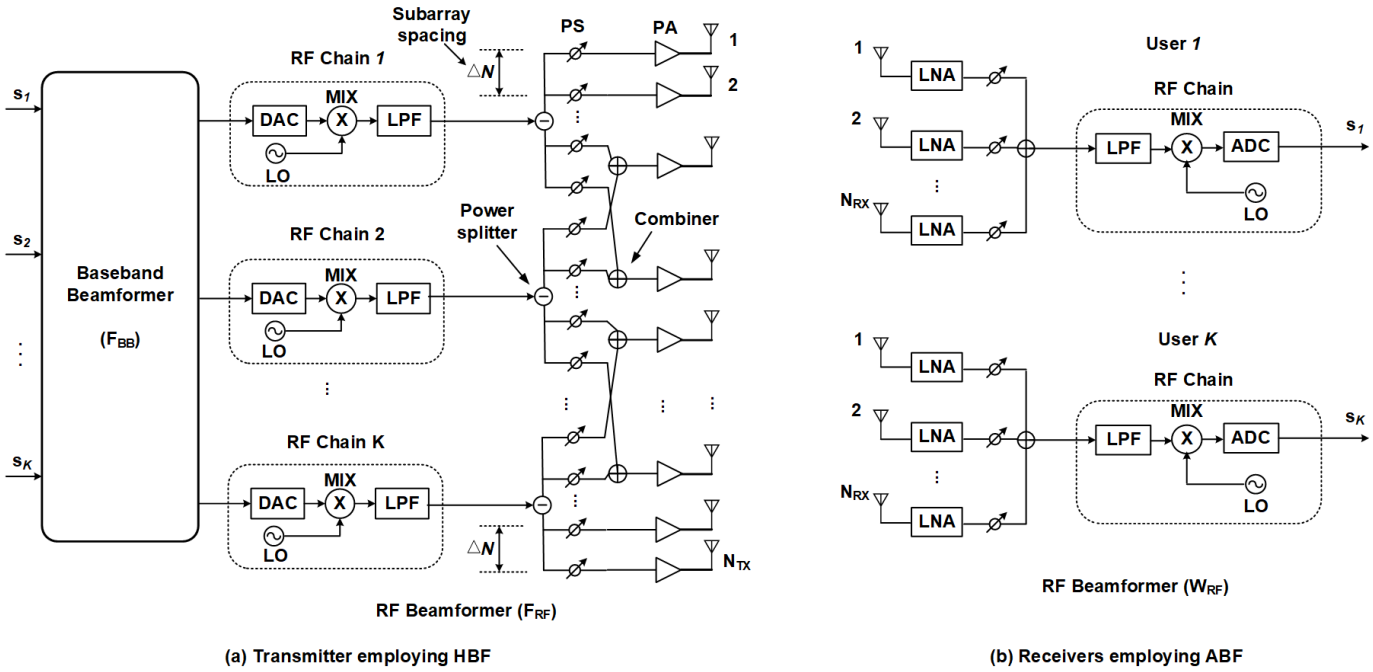

Figure 1. Beamforming Array Structure

precoding and postcoding techniques employed in Section IV. Simulation results and discussions follow in Section V, while conclusion and the future research direction are presented in section VI.

Notations: We use the following notations throughout the paper. $\mathbf{A}$ is a matrix, $\mathbf{a}$ is a vector and a is a scalar. The identity and block diagonal matrices are denoted with $\mathbf{I}$ and $blkdiag$, respectively. $|\cdot|$ represents the cardinality of a vector, $\|\cdot\|_F$ denotes the Frobenius norm and $[\mathbf{A}]_{m,n}$ represents the element of matrix $\mathbf{A}$ in the m^{th} row and n^{th} column. The inverse, transpose and conjugate transpose operator are denoted with $(\cdot)^{-1}$, $(\cdot)^T$ and $(\cdot)^H$, respectively.

II. Generalized HBF Array Structure

In this section, we describe the generalized model for the HBF array structure proposed in this work as shown in Fig. 1(a). We first outline the step-wise procedures for the design of the generalized framework and then introduce a realistic power consumption model for the HBF architecture.

A. Design Procedures

(i) Set the transmit power (P_T) for the BS, noting the appropriate regulation on the effective isotropic radiated power (EIRP) limits.

(ii) Set the number of AEs (N_{TX}) for the BS of the massive MIMO system under consideration.

(iii) Determine the number of RF chains (N_{RF}) based on the expected maximum multiplexing capability of the BS. Note that for any HBF structure, $1 < N_{RF} < N_{TX}$.

(iv) Set the inter-subarray spacing $(\triangle N)$ where $\triangle N \in \left\{0, 1, 2, \ldots, \frac{N_{TX}}{N_{RF}}\right\}$. For the generalized framework proposed in this work, note that $\triangle N$ is the critical parameter that determines the specific array structure, as given by (1).

$$\triangle N = \begin{cases} 0 & \rightarrow fully-connected \\ \left[1, \frac{N_{TX}}{N_{RF}} - 1\right] & \rightarrow overlapped \\ \frac{N_{TX}}{N_{RF}} & \rightarrow sub-connected \end{cases} \quad (1)$$

(v) Determine the required number of PSs for each RF chain $\left(N_{PS}^k, \quad \forall k \in \{1, 2, \ldots, N_{RF}\}\right)$ using (2). The total number of required PSs (N_{PS}) for a BS is then determined using (3).

$$N_{PS}^k = N_{TX} - \triangle N\left(N_{RF} - 1\right) \quad (2)$$

$$N_{PS} = \sum_{k=1}^{N_{RF}} N_{PS}^k = N_{RF} \times N_{PS}^k \quad (3)$$

(vi) For each RF chain, develop the mapping index vector $\mathbf{m}_k$ using (4) where $\forall k \in \{1, 2, \ldots, N_{RF}\}$. The entries in $\mathbf{m}_k$ give the indices of the AEs connected to the k^{th} RF chain.

$$\mathbf{m}_k = \left[(k-1) \triangle N + 1, \ldots, N_{TX} - \triangle N\left(N_{RF} - k\right)\right] \quad (4)$$

Note that the number of AEs in a subarray $\left(N_{sub}^{TX}\right)$ equals the number of PSs connected to each RF chain, where $N_{sub}^{TX} = N_{PS}^k = |\mathbf{m}_k|$.

(vii) Develop the $N_{TX} \times N_{RF}$ mapping index matrix $(\mathbf{M})$ by stacking the $\mathbf{m}_k$'s. Elements of $\mathbf{M}$ are given by (5) and each element shows the connection index of

the k^{th} RF chain to the j^{th} AE, $\forall k \in \{1, 2, \ldots, K\}$, $\forall j \in \{1, 2, \ldots, J\}$ by letting $K = N_{RF}$ and $J = N_{TX}$. We note that $\mathbf{M}$ becomes a $blkdiag$ matrix for the sub-connected array structure.

$$\mathbf{M} = \begin{bmatrix} m_{1,1} & \mathbf{0} & \cdots & \mathbf{0} \\ \vdots & m_{\triangle N+1,2} & \cdots & \mathbf{0} \\ m_{N_{sub},1} & \vdots & \cdots & m_{J-N_{sub}+1,K} \\ \mathbf{0} & m_{\triangle N+N_{sub},2} & \ddots & \vdots \\ \mathbf{0} & \mathbf{0} & \mathbf{0} & m_{J,K} \end{bmatrix} \tag{5}$$

(viii) Develop the $N_{TX} \times N_{RF}$ (or $J \times K$) boolean/binary matrix $\mathbf{B}$ by replacing all nonzero elements of $\mathbf{M}$ in (5) with ones ($\mathbf{1's}$) as shown in (6).

$$\mathbf{B} = \begin{bmatrix} 1 & \mathbf{0} & \cdots & \mathbf{0} \\ \vdots & 1 & \cdots & \mathbf{0} \\ 1 & \vdots & \cdots & 1 \\ \mathbf{0} & 1 & \ddots & \vdots \\ \mathbf{0} & \mathbf{0} & \mathbf{0} & 1 \end{bmatrix} \tag{6}$$

(ix) Develop the $N_{TX} \times 1$ combiner vector ($\mathbf{g}$), given by (7) indicating the number of RF chains connected to the j^{th} AE.

$$\mathbf{g} = \begin{bmatrix} g_1 \\ g_2 \\ \vdots \\ g_{N_{TX}} \end{bmatrix}, \qquad g_j = \sum_{k=1}^{N_{RF}} \mathbf{B}_{j,k} \quad \forall j \in \{1, 2, \ldots, N_{TX}\} \tag{7}$$

(x) Determine the number of combiners (N_{comb}) needed for the specific array structure using (8). Note that AEs connected to just a single RF chain do not need combiners.

$$N_{comb} = \left| [g_j > 1]_{j=1}^{N_{TX}} \right| = \begin{cases} N_{TX} & \rightarrow fully - connected \\ N_{TX} - 2 \triangle N & \rightarrow overlapped \\ 0 & \rightarrow sub - connected \end{cases} \tag{8}$$

(xi) Determine the transmit beam power $\left(P_b^k\right)$ for each of the K beams using (9) where $(\cdot)$ is the weighting factor. The total transmit power constraint set in step (i) is enforced by (10).

$$P_b^k = \frac{P_T}{N_{TX}} \left(\sum_{j \in \mathbf{m}_k} (g_j)^{-1} \right) \tag{9}$$

$$P_T = \sum_{k=1}^{N_{RF}} P_b^k \tag{10}$$

Based on the enumerated design procedures, the required number of components for the different subarray configurations can be determined depending on the choice of $\triangle N$. We remark that while the design procedures outlined above focus on the BS or AP, the generalized framework is equally applicable for the RXs or UEs by replacing the appropriate TX components with the corresponding RX components. A table such as Table I can then be populated with the appropriate entries based on the values set and determined in this subsection.

In Table I, we give the values of the required number of components for the sample scenario considered in this work where the AP is equipped with $N_{TX} = 64$, $N_{RF}^{TX} = 8$ and $\triangle N = \{0, 2, 4, 6, 8\}$. The AP employs the generalized structure as shown in Fig. 1. This leads to the fully-connected structure when $\triangle N = 0$ and leads to the sub-connected structure when $\triangle N = N_{TX}/N_{RF}$ while $\triangle N = \{1, 2, \cdots, N_{TX}/N_{RF} - 1\}$ represent the overlapped subarray structure. For the UEs, we consider $N_{RX} = 8$, $N_{RF}^{RX} = 1$ and $\triangle N = 0$ for all the users $K = \{1, 2, \cdots, 8\}$. This corresponds to a fully-connected structure for the single stream per user ABF configuration. The numbers of the respective required components for each UE are also given in Table I.

B. Power Consumption Model

The power consumption model of the generalized HBF array structure in Fig. 1 is given in this subsection. We model a realistic power consumption framework considering not only the power consumption at the radio access network P_{RAN} but also the backhaul power consumption P_{BH}. The total consumed power P_{total} is thus given by (11).

$$P_{total} = P_{RAN} + P_{BH} \tag{11}$$

(i) RAN Power (P_{RAN}): For the coverage of a single BS, P_{RAN} consists of the transmit power of the BS P_T, the circuit power of the BS P_{cct}^{TX} and the combined RX circuit powers P_{cct}^{RX} of all the N_{UE} users served by the BS. Different from most existing studies [5], [11], [22], we include the power consumed by the RXs in the model.

$$P_{RAN} = P_T + P_{cct}^{TX} + N_{UE}\left(P_{cct}^{RX}\right) \tag{12}$$

(ii) Backhaul Power (P_{BH}): This involves the power consumed for the communication between the BS and the core network. It is dependent on the data rate (R) or the amount of data transferred per unit time ($bits/s$). In (13), $L_{BH} = 250$ mW/(Gbits/s) [21] is the power per unit data rate.

$$P_{BH} = L_{BH} \cdot R \tag{13}$$

The breakdown of the component powers, their values and number of required components are given by (16)-(18) (on the top of the next page), and in Table I and Table II, respectively. We assume a fixed miscellaneous power $P_{FIX} = 1$ W (noting that small cell BSs or APs do not have an active cooling

Table I
HBF ARRAY STRUCTURE COMPONENTS

TX Component	$\triangle N=0$	$\triangle N=2$	$\triangle N=4$	$\triangle N=6$	$\triangle N=8$	RX Component	$\triangle N=0$
N_{TX}	64	64	64	64	64	N_{RX}	8
N_{PA}	64	64	64	64	64	N_{LNA}	8
N_{RF}	8	8	8	8	8	N_{RF}	1
N_{sub}	64	50	36	22	8	N_{sub}	8
N_{PS}	512	400	288	176	64	N_{PS}	8
N_{comb}	64	60	56	52	0	N_{comb}	0

Table II
POWER CONSUMPTION OF COMPONENTS

TX Component	Unit Power Consumption	Value [mW]	RX Component	Unit Power Consumption	Value [mW]
P_{DAC}	Digital to Analog Converter [20]	110	P_{ADC}	Analog to Digital Converter [20]	200
P_{MIX}	Mixer [5]	23	P_{MIX}	Mixer [5]	23
P_{LO}	Local Oscillator [5]	5	P_{LO}	Local Oscillator [5]	5
P_{LPF}	Low Pass Filter [5]	15	P_{LPF}	Low Pass Filter [5]	15
P_{PS}	Phase Shifter [20]	30	P_{PS}	Phase Shifter [20]	30
P_{PA}	Power Amplifier [20]	16	P_{LNA}	Low Noise Amplifier [20]	30
P_{BB}	Baseband precoder [20]	243	-	-	-
P_{comb}	Combiner [21]	19.5	-	-	-

$$P_{cct}^{TX} = N_{RF}^{TX} P_{RFC}^{TX} + N_{RF}^{TX} N_{sub}^{TX} P_{PS}^{TX} + N_{TX} P_{PA} + N_{comb}^{TX} P_{comb}^{TX} + P_{BB}^{TX} + P_{FIX} \tag{16}$$

$$P_{cct}^{RX} = N_{RF}^{RX} P_{RFC}^{RX} + N_{RF}^{RX} N_{sub}^{RX} P_{PS}^{RX} + N_{RX} P_{LNA} \tag{17}$$

$$\begin{aligned} P_{total} =& P_T + \left[N_{RF}^{TX} P_{RFC}^{TX} + N_{RF}^{TX} N_{sub}^{TX} P_{PS}^{TX} + N_{TX} P_{PA} + N_{comb}^{TX} P_{comb}^{TX} + P_{BB}^{TX} + P_{FIX}\right] \\ & N_{UE}\left[N_{RF}^{RX} P_{RFC}^{RX} + N_{RF}^{RX} N_{sub}^{RX} P_{PS}^{RX} + N_{RX} P_{LNA}\right] + L_{BH} \cdot R \end{aligned} \tag{18}$$

system [23]). The P_{RFC}^{TX} and P_{RFC}^{RX} are given by (14) and (15), respectively [5].

$$P_{RFC}^{TX} = P_{DAC} + P_{MIX} + P_{LO} + P_{LPF} \tag{14}$$

$$P_{RFC}^{RX} = P_{ADC} + P_{MIX} + P_{LO} + P_{LPF} \tag{15}$$

III. C-I2X Application Scenario

Notwithstanding the benefits that can be harnessed with THz massive MIMO, the use cases identified for THzBC are still largely limited to short-range communication scenarios. These ultra-high rate applications include terabit wireless local area network (T-WLAN), terabit wireless personal area network (T-WPAN) and on-chip/chip-to-chip communications [4]. For outdoor applications, research trends point to the viability of THzBC for cellular and vehicular networks [1]. In these two scenarios, THz access points (APs) mounted on street lampposts can be used to provide ultra-broadband connectivity to pedestrian cellular users as well as high-mobility vehicles [6], [24]. The inter-site distance (ISD) of the THz APs in such scenarios typically does not exceed 10 m due to the high path loss (PL) at THz frequencies.

The range constraint of THzBC necessitates the ultra-dense deployment of transceivers thereby leading to the Dense Terahertz Massive MIMO Networks, referred to as DenseTeraNet throughout this paper. DenseTeraNet mimics the 5G ultra-dense small cell network (UDN) framework and inherits its benefits and challenges, both features at a much larger scale.

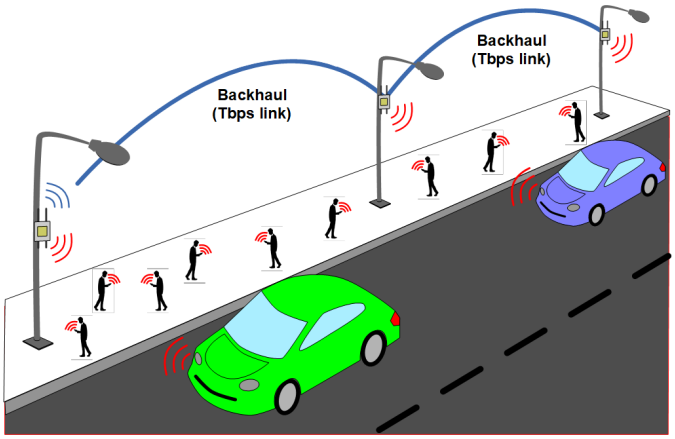

Figure 2. System deployment for C-I2X

The application scenario is shown in Fig. 2 where we consider DenseTeraNet for a cellular infrastructure to everything (C-I2X) paradigm. 'X' represents a combination of pedestrian users and high-mobility vehicles while 'I' refers the lamppost-mount AP for the downlink communication scenario.

The DenseTeraNet model is a promising candidate to offload traffic from the base stations (BSs) and provide enhanced mobile broadband (eMBB) to users in the context of cellular communications. In a similar vein, it will also support the cellular vehicle to anything (C-V2X) paradigm for next-generation vehicular networks (NGVNs). Towards 5G/B5G, the third generation partnership project (3GPP) is pushing the limits for cellular networks while the fifth generation Automotive Association (5GAA) is driving the efforts for the commercialization of the 5G New Radio (NR) C-V2X. The partnership of the key players in the automotive and telecommunications industries aims to evolve innovative technology solutions for the future intelligent transport systems (ITS) and next-generation mobile networks (NGMN) [24].

While both the eMBB [25] and the 5G NR C-V2X [24] use cases require ultra-high rate communication, the legacy dedicated short range communication (DSRC) and the Long Term Evolution Advanced (LTE-A) can only support maximum rates of 27 and 100 Mbps, respectively [6]. These rates are grossly inadequate for the above B5G use cases foreseen to require multi-Gbps or Tbps rates. Similar challenges are foreseen with regards to the bandwidth, reliability and latency requirements. Consequently, THzBC is being identified to come to the rescue. Typical applications of the DenseTeraNet C-I2X will include autonomous driving, high-rate infotainment and ultra-reliable safety services, among others [6], [24].

B5G mobile devices and ITS-supported vehicles will, therefore, be equipped with arrays of sensors that will generate terabytes of data. On-board communication chipsets will facilitate the use and sharing of this data for diverse services and applications such as live map download, videos streaming, cloud processing, cooperative perception, platooning, intent/trajectory sharing, real-time local updates, path planning, collision avoidance, blind-spot removal and general warnings. Overall, these features will lead to enhanced vehicular safety, better traffic management, more efficient toll collection, commute time reduction and ultra-broadband connectivity for increased quality of experience (QoE) of users.

IV. System Model

Consider the network deployment layout shown in Fig. 2. We focus on the single-cell, multi-user downlink scenario where a massive MIMO AP communicates N_{UE} user devices (i. e., the sum of cellular and vehicular users being scheduled in each transmission time interval (TTI)). Using the generalized structure introduced in Section II, we consider an AP employing HBF (with $N_{TX} = 64$, $N_{RF}^{TX} = 8$). At the UEs, we consider ABF (i.e., where $N_{RX} = 8$, $N_{RF}^{RX} = 1$ at each UE) thereby focusing on the multi-user beamforming case with a single stream per user, as shown in Fig. 1. The total number of streams $N_s = N_{UE} = N_{RF}^{TX} = 8$. All other necessary parameters and components have been introduced, defined and determined in Section II, and in particular in Tables I and II.

A. THz Channel Model

As shown in the network layout in Fig. 2, we consider an urban street deployment where the APs are mounted on street lampposts along a road 500 m long. The APs are evenly spaced at 10 m interval and are mounted at a height $h_{TX} = 5$ m on the walkway lampposts. All UEs are at a height of $h_{RX} = 1.5$ m. Each cellular user (cUE) traverses the route at a pedestrian speed of $v_{RX}^{c} = 3.6$ km/h while each vehicular user (vUE) moves at $v_{RX}^{v} = 36$ km/h, respectively. The width (w) of the walkway for cUEs is 2 m while the vUEs are at a further 3 m from the walkway. At each time instant, the I2X downlink connectivity is by line of sight (LoS) as the three-dimensional (3D) separation distance (d) between each user and its serving AP gives a LOS probability $P_{LOS} \approx 1$, according to (19) [26].

$$P_{\mathrm{LOS}}(d) = \left[\min\left(\frac{27}{d}, 1\right)\left(1 - e^{-\frac{d}{71}}\right) + e^{-\frac{d}{71}}\right]^2 \quad (19)$$

We consider a 3D statistical spatial channel model (SSCM) for the THz channel model. The large-scale fading is given by the effective omnidirectional path loss PL_{eff} which combines the path loss (PL) and the shadow fading (SF) as (20).

$$PL_{eff} = 20\log_{10}\left(\frac{4\pi f_c}{c}\right) + 10\bar{n}\log_{10}(d) + X(0,\sigma) \quad (20)$$

where $\bar{n}$ is the path loss exponent (PLE) and X is the log-normal random SF variable with zero mean and σ standard deviation.

For the small-scale fading, we consider a single-path channel for analytical tractability. Accordingly, the double-directional channel impulse response (CIR) h_{dir} for the transmission link of each UE is given by (21).

$$h_{dir}(t,\phi,\theta) = P_{RX} \cdot e^{j\varphi} \cdot \delta(t-\tau) \cdot G_{TX}(\phi,\theta) \cdot G_{RX}(\phi,\theta) \quad (21)$$

For the single-path channel in (21), P_{RX}, φ and τ denote the received power magnitude, phase and propagation time delay, respectively. The time is t while ϕ and θ are the angle offsets from the boresight direction for the azimuth and elevation, respectively. It is instructive to note that for a single-path LoS channel, the offsets $(\phi,\theta) = 0$ as the angles of departure (AoD) are the same as the boresight angles, for both the azimuth and elevation. $G_{TX}(\phi,\theta)$ and $G_{RX}(\phi,\theta)$ are the TX and RX antenna array gains that are modeled with (22) and (23) [26].

$$G_{TX/RX}(\phi,\theta) = \max\left(G_0 e^{\alpha\phi^2+\beta\theta^2}, \frac{G_0}{100}\right) \quad (22)$$

$$G_0 = \frac{41253\xi}{\phi_{3dB}^2\theta_{3dB}^2}, \quad \alpha = \frac{4\ln(2)}{\phi_{3dB}^2}, \quad \beta = \frac{4\ln(2)}{\theta_{3dB}^2} \quad (23)$$

where G_0 is the maximum directive boresight gain, ξ is the average antenna efficiency, ϕ_{3dB} and θ_{3dB} are the azimuth and elevation half-power beamwidths (HPBW), respectively. The variables α and β are evaluated using (23). Further, G_{TX} and G_{RX}, as well as the corresponding $\left(\phi_{3dB}^{TX}, \theta_{3dB}^{TX}\right)$ and $\left(\phi_{3dB}^{RX}, \theta_{3dB}^{RX}\right)$, are determined by the number of AEs forming a beam N_{sub}. As $\triangle N$ increases, N_{sub} decreases (see Table I). Consequently, as we move from the fully-connected, through the overlapped subarray, to the subconnected array,

the array gain G decreases. Given that G_{AE} is the gain of an antenna element, G_{TX} and G_{RX} are given by (24) and (25), respectively [27].

$$G_{TX}(dB) = G_{AE}(dB) + 10\log_{10}(N_{sub}^{TX}) \tag{24}$$

$$G_{RX}(dB) = G_{AE}(dB) + 10\log_{10}(N_{sub}^{RX}) \tag{25}$$

Note that with mobility, the phase (φ) is composed of the distance-dependent phase change (Φ) and the velocity-induced Doppler shift (ϑ_D) which is given by (26)-(28).

$$\varphi = \Phi + \vartheta_D \tag{26}$$

$$\varphi = 2\pi\left(f_c\tau + f_D\Delta t\right) \tag{27}$$

$$\varphi = 2\pi\left(f_c\tau + \frac{v_{RX}\cos(\phi)}{\lambda}\Delta t\right) \tag{28}$$

where $\lambda = c/f_c$ is the wavelength, $c = 3\times10^8$ m/s is the speed of light, v_{RX} is user speed and f_D is the Doppler frequency which is positive when the user is moving towards the AP and negative when moving away from it [28].

For the sake of simplicity, we consider the uniform linear array (ULA) structure at both the AP and the UEs. The inter-element spacing is $d_{TX} = d_{RX} = \lambda/2$. The channel between an AP and each UE can be given by (29).

$$\mathbf{H} = \sqrt{N_{TX}N_{RX}PL(d)}\cdot e^{j2\pi\varphi}\cdot\mathbf{a}_{RX}\left(\phi^{RX}\right)\cdot\mathbf{a}_{TX}^{H}\left(\phi^{TX}\right) \tag{29}$$

where $\mathbf{a}_{TX}$ and $\mathbf{a}_{RX}$ in (29) are the TX and RX array response vectors given by (30) and (31), respectively [8], [26].

$$\mathbf{a}_{TX}\left(\phi^{TX}\right) = \frac{1}{\sqrt{N_{TX}}}\begin{pmatrix} e^{j\frac{2\pi}{\lambda}d_{TX}(n_t-1)\sin\left(\phi^{TX}\right)} \end{pmatrix} \quad \forall n_t = 1,2,\ldots,N_{TX} \tag{30}$$

$$\mathbf{a}_{RX}\left(\phi^{RX}\right) = \frac{1}{\sqrt{N_{RX}}}\begin{pmatrix} e^{j\frac{2\pi}{\lambda}d_{RX}(n_r-1)\sin\left(\phi^{RX}\right)} \end{pmatrix} \quad \forall n_r = 1,2,\ldots,N_{RX} \tag{31}$$

B. Precoding and Postcoding

Since HBF is considered at the TX, the AP uses a baseband precoder $\mathbf{F}_{BB} \in \mathbb{C}^{K\times K}$ in (32) followed by an RF precoder $\mathbf{F}_{RF} \in \mathbb{C}^{J\times K}$ given by (33) (where $J = N_{TX}$ and $K = N_{RF}^{TX} = N_{UE}$) such that [8]:

$$\mathbf{F}_{BB} = \left[\mathbf{f}_1^{BB}, \mathbf{f}_2^{BB}, \cdots, \mathbf{f}_K^{BB}\right] \tag{32}$$

$$\mathbf{F}_{RF} = \left[\mathbf{f}_1^{RF}, \mathbf{f}_2^{RF}, \cdots, \mathbf{f}_K^{RF}\right] \tag{33}$$

The transmit symbol vector $\mathbf{s} \in \mathbb{C}^{K\times1}$ and the sampled transmit signal vector $\mathbf{x} \in \mathbb{C}^{K\times1}$ in (34) are related by (35):

$$\mathbf{s} = [s_1, s_2, \cdots, s_K]^T, \qquad \mathbf{x} = [x_1, x_2, \cdots, x_K]^T \tag{34}$$

$$\mathbf{x} = \mathbf{F}_{RF}\mathbf{F}_{BB}\mathbf{s} \tag{35}$$

Since ABF is considered at each of the users, the RF postcoder $\mathbf{W}_{RF} \in \mathbb{C}^{N_{RX}\times K}$ is given by (36). The received signal vector (after the precoding and postcoding operations) is $\mathbf{y} = [y_1, y_2, \cdots, y_K]^T$ where y_k for each user $\forall k \in 1, 2, \cdots, K$ is given by (37).

$$\mathbf{W}_{RF} = \left[\mathbf{w}_1^{RF}, \mathbf{w}_2^{RF}, \cdots, \mathbf{w}_K^{RF}\right] \tag{36}$$

$$y_k = \mathbf{w}_k^H\mathbf{H}_k\sum_{k=1}^{K}\mathbf{F}_{RF}\mathbf{f}_k^{BB}s_k + \mathbf{w}_k^H n_k \tag{37}$$

In (37), $\mathbf{H}_k \in \mathbb{C}^{N_{RX}^k\times N_{TX}}$ is the channel matrix between the AP and the k^{th} UE and n_k is the additive white Gaussian noise (AWGN) following a complex normal distribution $CN(0,\sigma)$ with zero mean and σ standard deviation. The transmit power (P_T) constraint is realized by normalizing $\mathbf{F}_{BB}$ such that:

$$\|\mathbf{F}_{RF}\mathbf{F}_{BB}\|_F^2 = K \tag{38}$$

Since the RF precoder at the AP and the postcoder at each UE are implemented with PSs, elements (m,n) of $\mathbf{F}_{RF}$ and $\mathbf{W}_{RF}$ matrices are further constrained to have constant magnitudes (but variable phases). These constraints are enforced by (39) and (40). Therefore, the steering vectors based on the angles of AoD at the AP and AoA at each user are used as the RF beamformers for the precoder and postcoder, respectively [5], [8], [9].

$$[\mathbf{F}_{RF}]_{m,n} = \frac{1}{\sqrt{N_{TX}}}e^{j\phi_{m,n}} = \mathbf{a}_{TX}\left(\phi^{TX}\right) \tag{39}$$

$$[\mathbf{W}_{RF}]_{m,n} = \frac{1}{\sqrt{N_{RX}}}e^{j\phi_{m,n}} = \mathbf{a}_{RX}\left(\phi^{RX}\right) \tag{40}$$

For the baseband precoder $\mathbf{F}_{BB}$ at the AP, we employed the zero-forcing (ZF) precoder [29] given by (41) to cancel MUI. The effective channel $\mathbf{H}_{eff}^k$ (i.e., the equivalent channel after the RF precoding and postcoding operations) is given by (42).

$$\mathbf{F}_{BB} = \mathbf{H}_{eff}^H\left(\mathbf{H}_{eff}\mathbf{H}_{eff}^H\right)^{-1} \tag{41}$$

$$\mathbf{H}_{eff}^H = \mathbf{w}_k^H\mathbf{H}_k\mathbf{F}_{RF} \tag{42}$$

V. Spectral and Energy Efficiency Performance

Following the generalized HBF antenna structure and the system, channel and power consumption models introduced in Sections II-IV, we give the expressions for the performance of the system in this section, in terms of the achievable sum data rate (R), spectral efficiency (η_{SE}) and energy efficiency (η_{EE}). The main objective is to efficiently design $\mathbf{F}_{RF}$, $\mathbf{F}_{BB}$ and $\mathbf{W}_{RF}$ to maximize the system performance.

A. Spectral Efficiency and Achievable rate

Given the received signal y_k in (37), the η_{SE}^k [(bits/s)/Hz] and R_k (bits/s) of the k^{th} user are given by (43) and (44), respectively

$$\eta_{SE}^k = \log_2\left(1 + \frac{P_T^k \cdot \left|\mathbf{w}_k^H \mathbf{H}_k \mathbf{F}_{RF} \mathbf{f}_k^{BB}\right|^2}{\sum_{n \neq k} P_T^n \cdot \left|\mathbf{w}_k^H \mathbf{H}_k \mathbf{F}_{RF} \mathbf{f}_n^{BB}\right|^2 + \sigma_k^2}\right) \tag{43}$$

$$R_k = BW_k \times \eta_{SE}^k \tag{44}$$

where BW_k is the bandwidth allocated to the k^{th} user. Similarly, σ_k^2 is the noise term of the k^{th} user. The achievable sum rate of all the K users is

$$R = \sum_{k=1}^{K} R_k \tag{45}$$

Different from most works in the literature where $P_T^k = \frac{P_T}{K}$, we note that this is simply not the case for P_T^k for the generalized framework explored in this work, particularly for the overlapped subarray structure as already given in (9).

B. Energy Efficiency

The energy efficiency (b/J, bits/Joule) of the system is the ratio of the system throughput or sum data rate R (given by (45)) to the total power consumption P_{total} (expressed as (18) in Section II).

$$\eta_{EE} = \frac{sum\ rate}{total\ power\ consumed} = \frac{R}{P_{total}} \tag{46}$$

The optimal EE as a function of the SE, $\eta_{EE}^*(\eta_{SE})$ is given according to the fundamental EE-SE relation [30] by (47)

$$\left|\frac{d\eta_{EE}^*(\eta_{SE})}{d\eta_{SE}}\right|_{\eta_{SE}=\frac{R}{BW}} = 0 \tag{47}$$

$\eta_{EE}^*(\eta_{SE}) = \max\left(\eta_{EE}(\eta_{SE})\right)$ is strictly quasiconcave in η_{SE} when P_{total} includes both the transmit power P_T and the circuit power P_{cct} [30], [31].

VI. Simulation Results

In this section, simulation results are provided to illustrate the system performance in terms of SE, EE and hardware cost, and to compare the performance of the different subarray configurations. The deployment parameters have been enumerated in Section IV. The other key simulation parameters are further given in Table III. In each run or channel realization, users are randomly deployed for the first TTI. Thereafter, each UE follows its mobility course (with respect to speed and direction) throughout subsequent TTIs. The results are averaged over the simulations runs and TTIs.

Table III
SIMULATION PARAMETERS

Parameter	Description	Value
f_c	Carrier frequency	0.1 THz
BW	Bandwidth	2 GHz
$X(\mu, \sigma)$	Shadow fading	(0, 7) dB
N_o	Noise power spectral density	-174 dBm/Hz
NF	Noise figure	6 dB
P_T	Transmit power	$[0.1, \cdots, 8]$ W
G_{AE}	Antenna element gain	8 dBi
$G_{TX,max}$ (24)	Maximum transmit gain	26 dBi
$G_{RX,max}$ (25)	Maximum receive gain	17 dBi
$nRuns$	Number of channel realizations	1000

A. Power and Hardware Costs

First, we provide a comparative performance analysis of the structures with respect to the hardware requirement and power consumption. In Table I (see Section II), we provided a breakdown of the hardware components needed to realize each of the structures for the case where $N_{TX} = 64, N_{RF}^{TX} = 8$ for the AP and $N_{RX} = 8, N_{RF}^{RX} = 1$ for each of the $K = 8$ UEs. For the phased array network, the number of required PSs N_{PS} changes significantly with the specific structure. In Fig. 3, we show how N_{PS} varies with the N_{RF} for a fixed N_{TX}.

With a $P_{PS} = 30$ mW per unit PS, the overlapped subarray structures offer a window of opportunity between the fully-connected and the sub-connected structures at the two extreme ends, in terms of power consumption. The case is similar with respect to the number of combiners N_{comb} required for each of the structures. However, the contribution of the PSs to the P_{total} is far greater than that of the combiner, both in terms of the number required as well as the unit component power cost as can be seen in Tables I and II, respectively. With respect to the overall power consumption of the network, Fig. 4 shows the P_{total} for the different structures as well as the proportions of the contributing components (i.e., the consumed power at the TX (P_{TX}), the consumed power at all RX (P_{RXs}) and the power consumed for backhauling (P_{BH})) when $P_T = 1$ W. Note that $P_{total} = P_{TX} + P_{RXs} + P_{BH}$, where P_T is included in P_{TX}.

From Fig. 4, it can be seen that P_{total} decreases as we move from the fully-connected ($\triangle N = 0$), through the overlapped subarray, to the sub-connected structure ($\triangle N = 8$). Similarly, as we move from ($\triangle N = 0 \rightarrow \triangle N = 8$), the contribution of P_{TX} and P_{BH} reduces, with P_{TX} reducing at a faster rate than P_{BH}. Except for the fully-connected structure, $P_{BH} > P_{TX}$ for all structures. As noted in [23], the computation and backhaul power consumption will constitute the largest of the total power consumption of future networks. For all cases, the P_{RXs} maintain steady values, constituting roughly 10% and 15% of P_{total} for the fully-connected and sub-connected structures, respectively.

B. Spectral and Energy Efficiency

The sum SE and the EE performance for different transmit powers P_T, for all the considered structures, are shown in Figs. 5 and 6, respectively. For all the subarray structures in

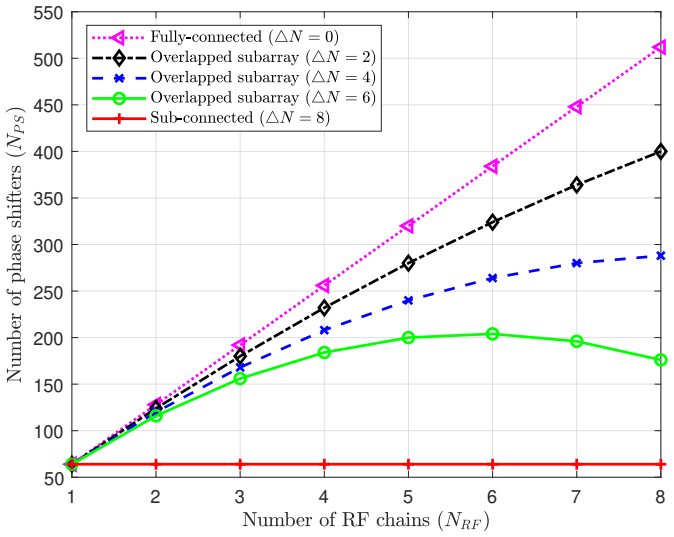

Figure 3. Number of PSs required for different structures ($N_{TX} = 64$)

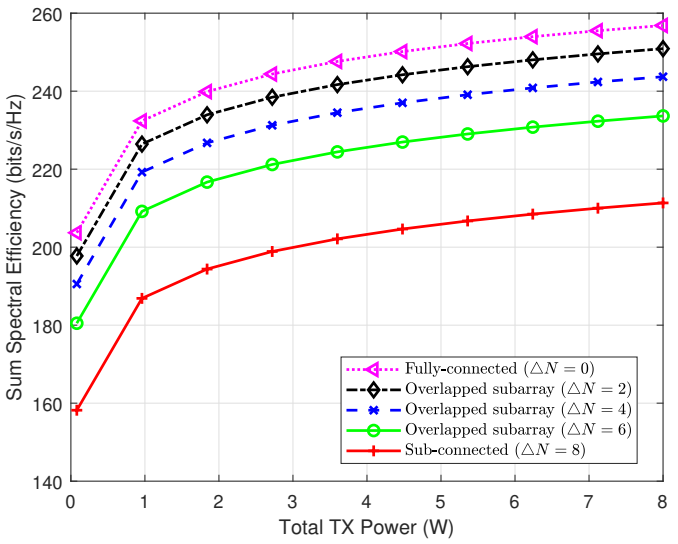

Figure 5. Sum Spectral efficiency versus total transmit power

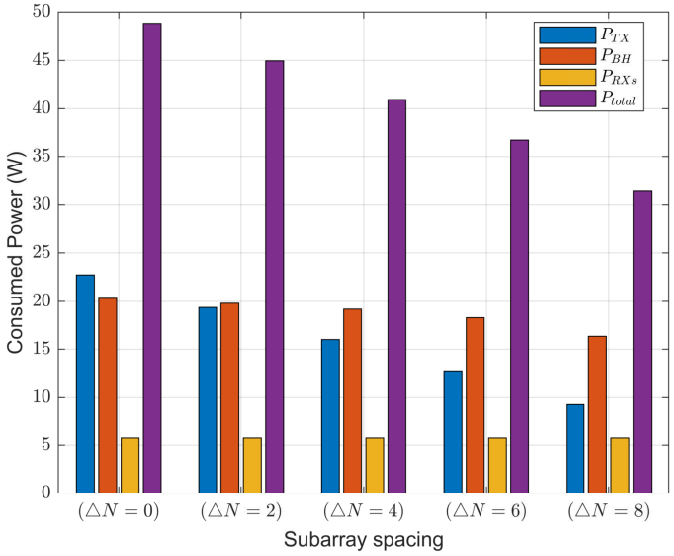

Figure 4. Power consumption of components for different $\triangle N$ ($P_T = 1$ W)

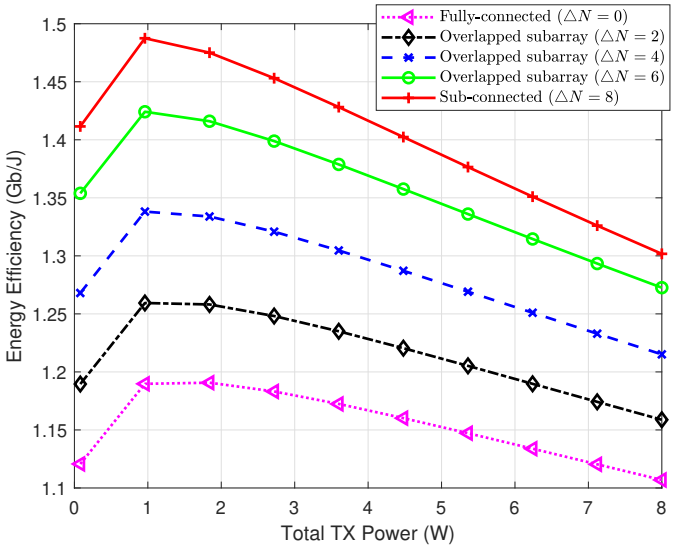

Figure 6. Energy efficiency versus total transmit power

Fig. 5, the SE increases logarithmically as P_T increases. The trend for the EE is however different. As shown in Fig. 6, the EE first increases, peaks (at the optimal value) and then decreases as P_T increases. The optimal EE point is critical for the design of energy-efficient networks, as the increase in P_T beyond the optimal value leads to performance degradation of the system with respect to the EE, though the SE continues to increase.

Fig. 7 shows the EE-SE performance tradeoff curves for the different subarray structures. For each structure, the EE starts to increase as the SE increases. It then reaches the optimal point (given by (47)) and thereafter continues to decrease as SE increases. Each curve follows a quasi-concave (bell-shaped) trend, which is consistent with the results in [5], [10], [30], [31]. Further, it can be observed that each of the structures has different performance. The fully-connected structure has the highest SE and lowest EE on one end, while the sub-connected structure has the lowest SE and highest EE on the other end. In between these two ends, the different overlapped subarray structures show varying performance depending on $\triangle N$. For example, the overlapped structure with $\triangle N = 4$ strikes a good balance in EE-SE performance for the considered scenario.

C. User Performance

In Fig. 8, we show the SE performance for all the users as the P_T increases. Similarly, the EE performance for all users with increasing P_T is shown in Fig. 9. For space constraints, we show the results for only the overlapped subarray case with $\triangle N = 4$ adjudged from the preceding subsection as the structure having a balanced performance tradeoff with respect to SE and EE.

In Figs. 8 and 9, it can be seen that the performance of each of the users are very close in values at each P_T point, thus guaranteeing a level of fairness among users. As usual,

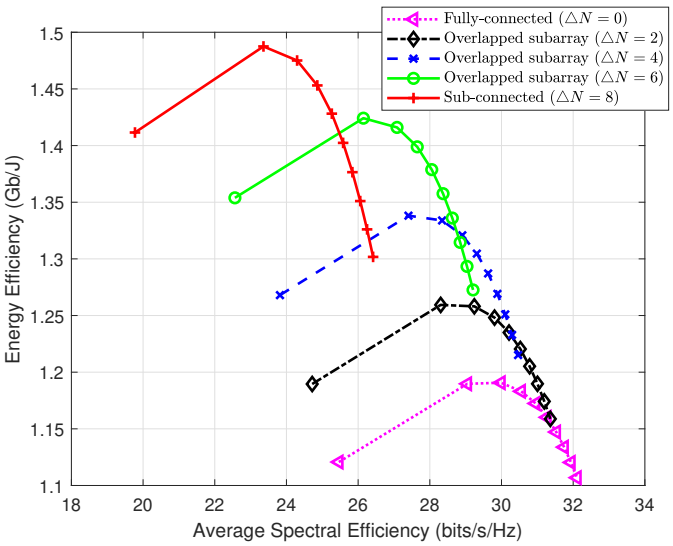

Figure 7. Energy efficiency versus spectral efficiency

Fig. 8 follows the logarithmically-increasing trend in SE as P_T increases for each of the users. Similarly, the curves in Fig. 9 follows the quasi-concave trend in EE as the P_T increases for each of the users. In addition, with equal bandwidth allocation per user, $R_k = \eta_{SE}^k \times (BW/K)$. Therefore, each user is able to reach a data rate of more than 5 Gbps (which is good for B5G) with a minimum SE of 20 bits/s/Hz in a 2 GHz BW for 8 users.

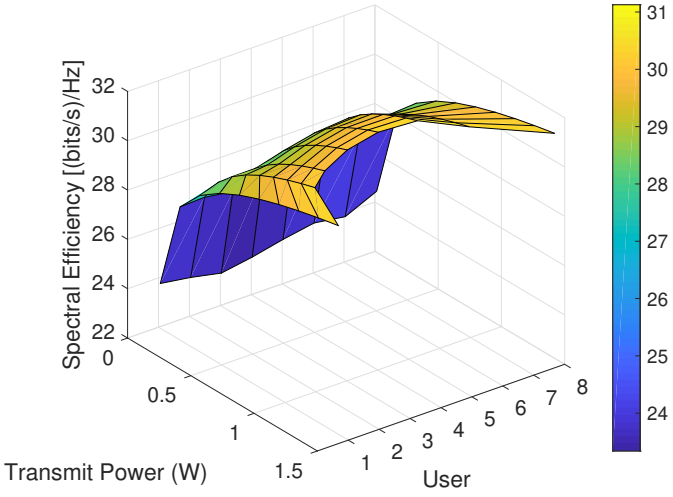

Figure 8. Spectral efficiency vs transmit power for each user ($\triangle N = 4$)

VII. Conclusion

In this paper, we proposed a novel generalized HBF array structure for the downlink THz multi-user massive MIMO network. The generalized framework enables the design and comparative performance analysis of different possible subarray configurations (i.e., the fully-connected, the sub-connected and the overlapped subarray structures). The performance of the proposed model was analyzed using a single-path LoS THz channel model for a C-I2X application scenario, where 'X' is

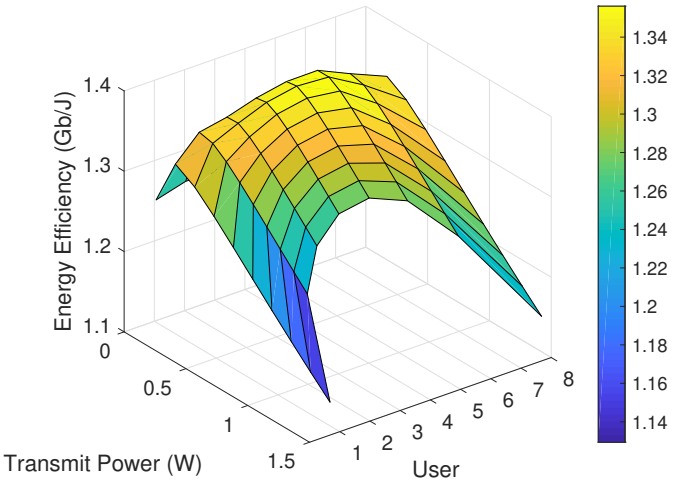

Figure 9. Energy efficiency vs transmit power for each user ($\triangle N = 4$)

combination of pedestrian users and high-mobility vehicles. The results show that the overlapped subarray structure can provide a balanced performance tradeoff in terms of SE, EE and hardware costs between the popular fully-connected structure (with high SE and limited EE) and the sub-connected structure (with reduced SE and high EE). The overlapped subarray structure, therefore, shows exciting potentials for next-generation networks that target both high-rate and green operation of networks. As a future work, it is of interest to extend the analysis to the multi-path channels and to a multi-cell scenario taking into consideration the effects of dense deployment of infrastructure.

References

[1] S. Mumtaz, J. M. Jornet, J. Aulin, W. H. Gerstacker, X. Dong, and B. Ai, "Terahertz Communication for Vehicular Networks," *IEEE Transactions on Vehicular Technology*, vol. 66, no. 7, pp. 5617–5625, July 2017.

[2] K. M. S. Huq, J. M. Jornet, W. H. Gerstacker, A. Al-Dulaimi, Z. Zhou, and J. Aulin, "THz Communications for Mobile Heterogeneous Networks," *IEEE Communications Magazine*, vol. 56, no. 6, pp. 94–95, June 2018.

[3] S. A. Busari, K. M. S. Huq, S. Mumtaz, and J. Rodriguez, "Terahertz Massive MIMO for Beyond-5G Wireless Communication," in *2019 IEEE International Conference on Communications (ICC)*, Shanghai, P.R. China, May 2019, pp. 1–6.

[4] I. F. Akyildiz, J. M. Jornet, and C. Han, "Terahertz band: Next frontier for wireless communications," *Physical Communication*, vol. 12, pp. 16–32, 2014.

[5] C. Lin and G. Y. Li, "Energy-Efficient Design of Indoor mmWave and Sub-THz Systems With Antenna Arrays," *IEEE Transactions on Wireless Communications*, vol. 15, no. 7, pp. 4660–4672, July 2016.

[6] V. Va, T. Shimizu, G. Bansal, and R. W. H. Jr., "Millimeter Wave Vehicular Communications: A Survey," *Foundations and Trends in Networking*, vol. 10, no. 1, pp. 1–113, 2016.

[7] S. A. Busari, K. M. S. Huq, S. Mumtaz, L. Dai, and J. Rodriguez, "Millimeter-Wave Massive MIMO Communication for Future Wireless Systems: A Survey," *IEEE Communications Surveys & Tutorials*, vol. 20, no. 2, pp. 836–869, Secondquarter 2018.

[8] A. Alkhateeb, G. Leus, and R. W. Heath, "Limited Feedback Hybrid Precoding for Multi-User Millimeter Wave Systems," *IEEE Transactions on Wireless Communications*, vol. 14, no. 11, pp. 6481–6494, Nov 2015.

[9] O. E. Ayach, S. Rajagopal, S. Abu-Surra, Z. Pi, and R. W. Heath, "Spatially Sparse Precoding in Millimeter Wave MIMO Systems," *IEEE Transactions on Wireless Communications*, vol. 13, no. 3, pp. 1499–1513, March 2014.

[10] S. A. Busari, K. M. S. Huq, G. Felfel, and J. Rodriguez, "Adaptive Resource Allocation for Energy-Efficient Millimeter-Wave Massive MIMO Networks," in *2018 IEEE Global Communications Conference (GLOBECOM 2018)*, Abu Dhabi, United Arab Emirates, Dec. 2018, pp. 1–6.

[11] X. Gao, L. Dai, S. Han, C. L. I, and R. W. Heath, "Energy-Efficient Hybrid Analog and Digital Precoding for MmWave MIMO Systems With Large Antenna Arrays," *IEEE Journal on Selected Areas in Communications*, vol. 34, no. 4, pp. 998–1009, April 2016.

[12] Z. Wang, J. Zhu, J. Wang, and G. Yue, "An Overlapped Subarray Structure in Hybrid Millimeter-Wave Multi-User MIMO System," in *2018 IEEE Global Communications Conference (GLOBECOM 2018)*, Abu Dhabi, United Arab Emirates, Dec. 2018, pp. 1–6.

[13] S. Kutty and D. Sen, "Beamforming for Millimeter Wave Communications: An Inclusive Survey," *IEEE Communications Surveys Tutorials*, vol. 18, no. 2, pp. 949–973, Secondquarter 2016.

[14] S. Han, C. l. I, Z. Xu, and C. Rowell, "Large-scale antenna systems with hybrid analog and digital beamforming for millimeter wave 5G," *IEEE Communications Magazine*, vol. 53, no. 1, pp. 186–194, Jan. 2015.

[15] X. Gao, L. Dai, Z. Gao, T. Xie, and Z. Wang, "Precoding for mmWave massive MIMO," in *mmWave Massive MIMO*, S. Mumtaz, J. Rodriguez, and L. Dai, Eds. Academic Press, 2017, pp. 79–111.

[16] N. Song, T. Yang, and H. Sun, "Overlapped Subarray Based Hybrid Beamforming for Millimeter Wave Multiuser Massive MIMO," *IEEE Signal Processing Letters*, vol. 24, no. 5, pp. 550–554, May 2017.

[17] O. E. Ayach, R. W. Heath, S. Rajagopal, and Z. Pi, "Multimode precoding in millimeter wave MIMO transmitters with multiple antenna sub-arrays," in *2013 IEEE Global Communications Conference (GLOBECOM)*, Dec 2013, pp. 3476–3480.

[18] N. Song, H. Sun, and T. Yang, "Coordinated Hybrid Beamforming for Millimeter Wave Multi-User Massive MIMO Systems," in *2016 IEEE Global Communications Conference (GLOBECOM)*, Dec 2016, pp. 1–6.

[19] S. Sun, T. S. Rappaport, and M. Shafi, "Hybrid beamforming for 5G millimeter-wave multi-cell networks," in *IEEE INFOCOM 2018 - IEEE Conference on Computer Communications Workshops (INFOCOM WKSHPS)*, April 2018, pp. 589–596.

[20] S. Buzzi and C. D'Andrea, "Are mmWave Low-Complexity Beamforming Structures Energy-Efficient? Analysis of the Downlink MU-MIMO," in *2016 IEEE Globecom Workshops (GC Wkshps)*, Dec 2016, pp. 1–6.

[21] A. Pizzo and L. Sanguinetti, "Optimal design of energy-efficient millimeter wave hybrid transceivers for wireless backhaul," in *2017 15th International Symposium on Modeling and Optimization in Mobile, Ad Hoc, and Wireless Networks (WiOpt)*, May 2017, pp. 1–8.

[22] K. M. S. Huq, S. Mumtaz, J. Bachmatiuk, J. Rodriguez, X. Wang, and R. L. Aguiar, "Green HetNet CoMP: Energy Efficiency Analysis and Optimization," *IEEE Transactions on Vehicular Technology*, vol. 64, no. 10, pp. 4670–4683, Oct 2015.

[23] X. Ge, J. Yang, H. Gharavi, and Y. Sun, "Energy Efficiency Challenges of 5G Small Cell Networks," *IEEE Communications Magazine*, vol. 55, no. 5, pp. 184–191, May 2017.

[24] S. A. Busari, M. A. Khan, K. M. S. Huq, S. Mumtaz, and J. Rodriguez, "Millimetre-wave massive MIMO for cellular vehicle-to-infrastructure communication," *IET Intelligent Transport Systems*, January 2019. [Online]. Available: https://digital-library.theiet.org/content/journals/10.1049/iet-its.2018.5492

[25] S. A. Busari, S. Mumtaz, S. Al-Rubaye, and J. Rodriguez, "5G Millimeter-Wave Mobile Broadband: Performance and Challenges," *IEEE Communications Magazine*, vol. 56, no. 6, pp. 137–143, June 2018.

[26] M. K. Samimi and T. S. Rappaport, "3-D Millimeter-Wave Statistical Channel Model for 5G Wireless System Design," *IEEE Transactions on Microwave Theory and Techniques*, vol. 64, no. 7, pp. 2207–2225, July 2016.

[27] S. Sun, T. S. Rappaport, M. Shafi, P. Tang, J. Zhang, and P. J. Smith, "Propagation Models and Performance Evaluation for 5G Millimeter-Wave Bands," *IEEE Transactions on Vehicular Technology*, vol. 67, no. 9, pp. 8422–8439, Sep. 2018.

[28] A. Goldsmith, *Wireless Communications*. Cambridge University Press, Cambridge, United Kingdom, 2005.

[29] Q. H. Spencer, A. L. Swindlehurst, and M. Haardt, "Zero-forcing methods for downlink spatial multiplexing in multiuser MIMO channels," *IEEE Transactions on Signal Processing*, vol. 52, no. 2, pp. 461–471, Feb 2004.

[30] C. Xiong, G. Y. Li, S. Zhang, Y. Chen, and S. Xu, "Energy- and Spectral-Efficiency Tradeoff in Downlink OFDMA Networks," *IEEE Transactions on Wireless Communications*, vol. 10, no. 11, pp. 3874–3886, November 2011.

[31] K. M. S. Huq, S. Mumtaz, J. Rodriguez, and R. Aguiar, "Overview of Spectral- and Energy-Efficiency Trade-off in OFDMA Wireless System," in *Green Communication for 4G Wireless Systems*, S. Mumtaz and J. Rodriguez, Eds. River Publishers, Aalborg, 2013.

Sherif Adeshina Busari (S'14) received the B.Eng. and M.Eng. degrees in electrical and electronics engineering from the Federal University of Technology Akure, Nigeria, in 2011 and 2015, respectively. He is currently pursuing the Ph.D. degree on the MAP-Tele doctoral program in Telecommunications (a joint program of the University of Minho, the University of Aveiro, and the University of Porto). He is a PhD student researcher with the Instituto de Telecomunicações, Aveiro, Portugal and an Assistant Lecturer with the Federal University of Technology, Akure, Nigeria. He has served as a reviewer for many IEEE journals as well as technical program committee member and reviewer for IEEE Globecom 2018 and BROADNETS'18. He received the best paper award at the 2018 IEEE Globecom workshop on ultra-high speed, low latency and massive connectivity communication for 5G/B5G. His research interests include wireless channel modeling, millimeter-wave communications, massive MIMO, radio resource management and optimization for 5G and beyond-5G mobile networks.

Kazi Mohammed Saidul Huq (SM'17) received the B.Sc. degree in computer science and engineering from the Ahsanullah University of Science and Technology, Bangladesh, in 2003, the M.Sc. degree in electrical engineering from the Blekinge Institute of Technology, Sweden, in 2006, and the Ph.D. degree in electrical engineering from the University of Aveiro, Portugal, in 2014. He is a Senior Research Engineer with the Mobile Systems Group, Instituto de Telecomunicações, Aveiro. He is one of the founding members of the IEEE 1932.1 Standard. He has authored several publications, including papers in high-impact international conferences and journals, a book, and book chapters. He is the Principal Investigator of the CMU-Portugal exploratory research project on THz system for Beyond 5G communication. His research activities include 5G paradigm, communication haul, D2D communication, energy-efficient wireless communication, higher frequency communication (mmWave, THz), radio resource management, and MAC layer scheduling.

Shahid Mumtaz (SM'16) received the M.Sc. degree in electrical and electronic engineering from the Blekinge Institute of Technology, Karlskrona, Sweden, and the Ph.D. degree in electrical and electronic engineering from the University of Aveiro. He was a Research Intern with Ericsson and Huawei Research Laboratories. He has over seven years of wireless industry experience and is currently a Senior Research Scientist and a Technical Manager with the Instituto de Telecomunicações Aveiro, 4TELL Group, Portugal. He has authored over 150 publications in international conferences, journals, and book chapters, as well as 3 book editorials. His research interests lie in the field of architectural enhancements to 3GPP networks (i.e., LTE-A user plane and control plane protocol stack, NAS, and EPC), 5G related technologies, green communications, cognitive radio, cooperative networking, radio resource management, cross-layer design, backhaul/fronthaul, heterogeneous networks, M2M and D2D communication, and baseband digital signal processing.

Jonathan Rodriguez (SM'13) received the masters degree in electronic and electrical engineering and the Ph.D. degree from the University of Surrey, U.K., in 1998 and 2004, respectively. In 2005, he became a Researcher with the Instituto de Telecomunicações, Portugal, and a Senior Researcher in 2008, where he established the 4TELL Research Group targeting next generation Mobile Systems with key interests on 5G, security, and antenna design. He has served as a Project Coordinator for major international research projects, which includes Eureka LOOP and FP7 C2POWER, whilst serving as a Technical Manager for FP7 COGEU and FP7 SALUS. He is currently leading the H2020-ETN SECRET project, a European Training Network on 5G communications. In 2015, he became an Invited Associate Professor with the University of Aveiro, Portugal, and the Honorary Visiting Researcher with the University of Bradford, U.K. Since 2017, he has been a Professor of mobile communications with the University of South Wales, U.K. He has authored over 480 scientific works, that includes nine book editorials. He has been a Chartered Engineer since 2013, and a fellow of the IET in 2015.

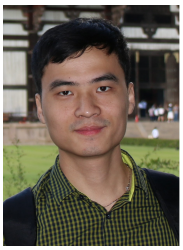

Yi Fang (M'15) received the B.Sc. degree in electronic engineering from East China Jiaotong University, China, in 2008, and the Ph.D. degree in communication engineering, Xiamen University, China, in 2013. From May 2012 to July 2012, He was a Research Assistant in electronic and information engineering, Hong Kong Polytechnic University, Hong Kong. From September 2012 to September 2013, he was a Visiting Scholar in electronic and electrical engineering, University College London, UK. From February 2014 to February 2015, he was a Research Fellow at the School of Electrical and Electronic Engineering, Nanyang Technological University, Singapore. He is currently an Associate Professor at the School of Information Engineering, Guangdong University of Technology, China. His research interests include information and coding theory, LDPC/protograph codes, spread-spectrum modulation, and cooperative communications. He is an Associate Editor of IEEE Access.

Douglas C. Sicker (M'90-SM'99) received his B.S., M.S., and Ph.D. degrees from the University of Pittsburgh. He was the DBC Endowed Professor with the Department of Computer Science, University of Colorado at Boulder with a joint appointment in, and the Director of, the Interdisciplinary Telecommunications Program. He is currently the Lord Endowed Chair of engineering, the Department Head of Engineering and Public Policy, and a Professor with the School of Computer Science, Carnegie Mellon University. He is also the Executive Director of the Broadband Internet Technical Advisory Group. He recently served as the Chief Technology Officer and a Senior Advisor for Spectrum with the National Telecommunications and Information Administration. He also served as the Chief Technology Officer of the Federal Communications Commission (FCC) and prior to this he served as a Senior Advisor on the FCC National Broadband Plan. He was the Director of Global Architecture at Level 3 Communications and served as the Chief of the Network Technology Division, FCC.

Saba Al-Rubaye (M'10-SM'17) received her Ph.D. in Electrical and Electronic Engineering from Brunel University London, UK. She is currently a Senior Lecturer in the School of Aerospace, Transport and Manufacturing at Cranfield University, UK. Dr. Al-Rubaye has more than 17 years of professional experience in the industry and academia with demonstrated track record of launching innovative solutions. Dr. Al-Rubaye has led and managed several research/industrial projects from conception to completion in Canada and USA. Prior to her current position, Dr. Al-Rubaye was working with advisory service on several integration, analysis and testing projects at Sustainable Technology Integration Laboratory (QT-STIL), Quanta Technology, Toronto, Canada. Before that she was, a senior researcher at Ryerson University, Canada and postdoctoral fellow at Stony Brook University, USA. Dr. Al-Rubaye is participating in developing industry standards by being an active research group member of IEEE P2784 Standard of Technology and Process Framework for Planning a Smart City, IEEE P1932.1 standard of License/unlicensed Interoperability and IEEE P1920.2, Standard for Vehicle to Vehicle Communications for Unmanned Aircraft Systems. Dr. Al-Rubaye has published many papers in IEEE journals and conferences, she is a recipient of the best technical paper award twice published in IEEE Vehicular Technology in 2011 and 2015, respectively. She served as technical program committee member for several prestigious conferences and workshops. Dr. Al-Rubaye is registered as a Chartered Engineer (CEng) by British Engineering Council and recognized as an Associate Fellow of the British Higher Education Academy (AFHEA) in the UK, she is a member of the Institute of Engineering and Technology (IET), and Senior Member of Institute of Electrical and Electronics Engineers (IEEE).

Antonios Tsourdos obtained a MEng on Electronic, Control and Systems Engineering from the University of Sheffield, an MSc on Systems Engineering from Cardiff University and a PhD on Nonlinear Robust Autopilot Design and Analysis from Cranfield University. He joined the Cranfield University in 1999 as lecturer, appointed Head of the Autonomous Systems Group in 2007 and professor of control engineering in 2009 and director of research in 2015. Professor Tsourdos was member of the Team Stellar, the winning team for the UK MoD Grand Challenge (2008) and the IET Innovation Award (Category Team, 2009).

2019-06-07

Generalized hybrid beamforming for vehicular connectivity using THz massive MIMO

Busari, Sherif Adeshina

IEEE

Busari SA, Haq KMS, Mumtaz S, Rodriguez J, Fang Y, Sicker DC, Al-Rubaye S and Tsourdos A., Generalized hybrid beamforming for vehicular connectivity using THz massive MIMO. IEEE Transactions on Vehicular Technology, Early online, June 2019

https://doi.org/10.1109/TVT.2019.2921563